Skewness Multi-Bernoulli-TBD Filter for Tracking Multiple Maneuvering Extended objects from ISAR Images

Mohamed Barbary[1], Mostafa Hamed[2]*, Julien Le Kernec[2]
[1] Electrical Engineering Department, Alexandria University, Egypt
[2]James Watt School of Engineering, University of Glasgow, Glasgow, UK
** m.elsayed.1@research.gla.ac.uk*

Keywords: Manoeuvring Extended objects, ISAR, Skew normal distribution Sub-random matrices model, MB-TBD filter

Abstract

The simultaneous imaging and tracking of manoeuvring extended objects (M-EOTs) is one of the most challenging problems in inverse synthetic aperture radar (ISAR) signal processing and has received significant attention recently. In this paper, we address multiple M-EOTs based on the track-before-detect (TBD) - Multi-Bernoulli (MB) approach, which is an efficient way to track low observable M-EOTs from ISAR images. To this end, we introduce a sub-Random Matrix Model (RMM)- MB-TBD composed of sub-ellipses; each one is represented by a RMM to denote the M-EOTs' extension. We also, propose a new ISAR observation model using a skewed (SK) normal distribution.

1 Introduction

IN recent years, detection and tracking of manoeuvring objects have attracted a lot of attention in the past decade and have played an increasingly important role in both military and civil fields [1-6]. Conventional maneuvering objects tracking methods consider point object that generates only one measurement for the object [2-3]. With the evolution of sensor technology, the focus of the object tracking literature shifted from point object tracking to extended object tracking (EOT) algorithms, which aim at estimating the object extent simultaneously with the kinematic state using a set of measurements per scan. The extent of an object can be considered as the region on the object's surface from which the measurements are obtained [1], [4-6]. The inverse synthetic aperture radar (ISAR) technique is an important tool for object recognition and classification; thus the high quality and real-time performance are two essential indicators for ISAR imaging [11-13]. Modern ISAR with high resolution, the EOT can be resolved into a series of scattering centers occupying different range cells in the received signal. Since ISAR contains abundant geometric and scattering information about the target extension including orientation, shape, and size. Throughout this study, we will focus on the maneuvering EOT (M-EOT) tracking from ISAR images. In this paper, we address a multiple M-EOTs Based on track-before-detect (TBD) approach, which is an efficient way to track low observable M-EOTs from ISAR images. Among the popular EOT approaches [1], [4-10], the random matrix model (RMM) approach appears promising since it is capable to jointly estimate the kinematic state and extension state without data association.

The RMM assumes an ellipse shape for the target's extent. These RMM methods perform well when scatter centers are symmetrically distributed around the centroid. For example, the distribution of these centers is uniform or Gaussian. However, in many real scenarios when a target maneuvers, the distribution over the whole EOT is not symmetric but skewed and distributed on some portions due to the unbalanced reflection of radar energy [14]. For ISAR radars, there are several factors that influence an EOT reflecting radar energy to the source, including the size, material, and orientation of the EOT, and the incident and reflected angles of the signal [14]. Different portions of an object can be made of various materials, and thus differ in abilities of reflection. Also, the incident and reflected angles can be different for portions of an object. All these factors lead to the phenomenon that measurement distribution is skewed. By consider that all of the kinematic state, extension, and skewness of ISAR measurement distribution may change when the EOT maneuvers. Moreover, further accurate data about orientation, shape, and size are extracted. However, only a single EOT tracker has been implemented so far. Thus, in [14], the authors presented an algorithm of EOTs tracking and estimated the non-linear kinematic state supported sub-RMM. To this point, we introduce a Sub-RMM-TBD composed of sub-ellipses; each one is represented by an RMM to denote the M-EOTs' extension and proposed a new ISAR observation model using a skew (SK) normal distribution. We organize the paper as follows. In Section II, we give a M-EOTs tracking problem from ISAR Images, in Section III the proposed algorithm, and the simulations results are given in Section IV. Section V contains conclusions.

2 Problem Formulation of Manoeuvering Extended Objects tracking from ISAR Images

During this work, multiple maneuvering extended object tracking (M-EOT) in the received raw data by ISAR was implemented using a Sub-RMM approach. In the following, we will explain the M-EOT signal, dynamic, and observation models supported by ISAR imaging with a Sub-RMM approach.

a. ISAR Image Model of Maneuvering Extended Objects

According to the synthetic aperture principle, the ISAR image is constructed by collecting the scattered field for different frequencies and look angles. That is, the received data are collected in the spatial-frequency domains, and then projected onto the XOY plane, as shown in Fig.1. As the convention of ISAR imaging, the M-EOT is often considered as an aggregation of strong scattering points, and the phase center O is generally selected as the geometry center of the object. Then in the geometric ISAR model, we assumed that the X axis, in the direction of the radar line of sight (RLOS), to be along the radial direction, and the Y axis in the azimuth direction. $P_n(x_n, y_n)$ is one of the N scattering points on the M-EOT, with Υ_n $(n = 1, \cdots, N)$ representing the backward scattering. Then the baseband signal describes as [11-13]

$$s(k) = \sum_{n=1}^{N} \Upsilon_n \exp\left[-j\frac{4\pi f_t}{c} R_n(k)\right] \tag{1}$$

where f_t is the transmitted frequency; c is the speed of light; and $R_n(k)$ is the instantaneous range from scattering point P_n to ISAR. By denote T_a as the observing duration, then $0 \le k \le T_a$. Therefore, in far-field objects $R_n(k) \approx R_k + x_n - y_n\theta_k$, where $(R_k = R_0 + \Delta_r)$ is the instantaneous range from the phase center of M-EOT to the radar, Δ_r is the range shift presented by the translational motion of M-EOT and R_0 is the initial range; θ_k is the instantaneous rotation angle. Practically, the successive baseband signal is often sampled along the fast-time (range) and the slow-time (cross-range/azimuth) dimension, to represent the relative discrete forms of the range direction and the azimuth direction. Assuming that the step frequency radar transmits a sequence of $\mathcal{N}$ bursts with transmitting interval T_B, and bandwidth B. Each burst consists of $\mathcal{M}$ narrow frequency band pulses with the pulse repetition interval T_s. The rotated angle of M-EOT is Ω; then the ISAR resolution can be expressed by the range resolution $(\delta_r = c/2B)$ and cross-range resolution $(\delta_{cr} = \lambda_c/2\Omega)$, where λ_c is the wavelength. ISAR image obtained by IFT after motion compensation as [11-13]:

$$ISAR(X,Y) = \int_{\Omega}\int_{B}\left[\sum_{n=1}^{N} \Upsilon_n \cdot e^{j\frac{4\pi f_t}{c}(X-x_n)} . e^{-j\frac{4\pi}{\lambda_c}(Y-y_n)\theta_k}\right] df_t\, d\theta_k$$
$$= \frac{4\pi\Omega}{c\lambda_c}\sum_{N} \Upsilon_n \operatorname{sinc}\left[\frac{2B}{c}(X-x_n), \frac{2\Omega}{\lambda_c}(Y-y_n)\right] \tag{2}$$

After sampling on the time-range domain, the observation array is delivered to the ISAR processor as an input signal, and it is processed to form the radar output image $\boldsymbol{Z}_k$. On the other hand, it is the input to the M-EOT processor.

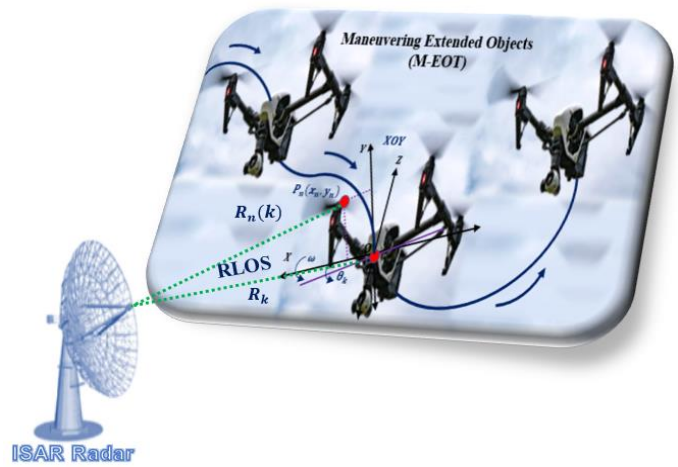

Fig.1. Geometry for ISAR imaging of manoeuvering extended object

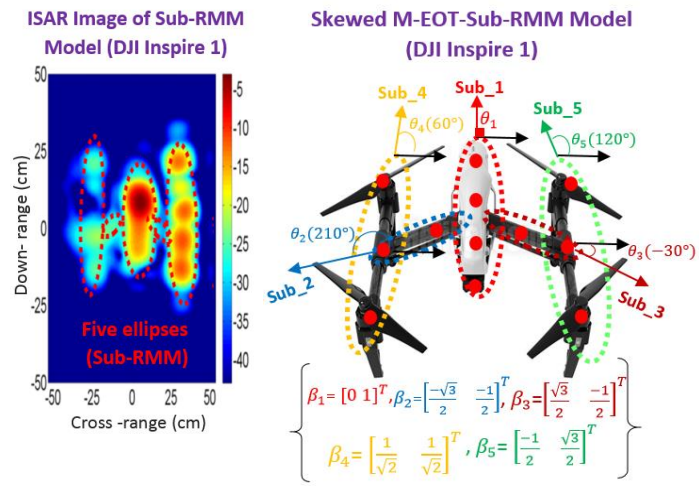

Fig.2. Illustration of approximating M-EOT (DJI Inspire 1) by using five Sub-ellipses, (left) ISAR images of M-EOT [11-13]; (right) Skewed M-EOT sub-RMM model with different $\theta_k^{(\ell,s)}$, $\beta_k^{(\ell,s)}$, the arrows show skewness direction

b. Dynamic model of Maneuvering EOT with sub-RMM

In the recent research works for EOT [1], [4-10], and [14], the EOT shape model is approximated by one ellipsoid using the RMM approach. In [4-5], [7], and [9], the authors used the many ellipsoids for each object, which are defined by the sub-ellipses or sub-RMM, to implement the object' extension within a linear dynamic model. This approximation is explained in Fig. 2 (left). The sub-RMM applied more detailed data about the shape, size, classification, orientation, and features of EOT. In this paper, we consider this approach of sub-RMM for the M-EOT. Let us consider at time k, the hybrid state $\boldsymbol{\xi}_k^{(\ell,s)}$is combining of the extension and kinematic states of an M-EOT using sub-RMM is defined by(3)

$$\mathbf{X}_k = \left\{\left\{\boldsymbol{\xi}_k^{(\ell,s)}\right\}_{s=1}^{n_k^{(\ell,s)}}\right\}_{\ell=1}^{N_{x,k}}, \quad \boldsymbol{\xi}_k^{(\ell,s)} \triangleq \left(\boldsymbol{x}_k^{(\ell,s)}, \boldsymbol{\chi}_k^{(\ell,s)}\right). \tag{3}$$

where $N_{x,k}$ is the number of M-EOTs, $n_k^{(\ell,s)}$ is the sub-RMM' number, $\boldsymbol{x}_k^{(\ell,s)} \in \mathbb{R}^{d_x}$ refer to be the kinematical model of sub-object s of ℓth M-EOT, $\boldsymbol{\chi}_k^{(\ell,s)} \in \mathbb{S}_{++}^{d}$ defines the extension state and $\mathbb{S}_{++}^{d}$ is represented by a set of $d \times d$ symmetric positive definite matrix (SPD), where d is the dimension of the M-EOT

extension. The kinematical state $\boldsymbol{x}_k^{(\ell,s)}$ Contains states related to sub-RMM kinematics, such as position, velocity, and heading. Thus, the maneuvering kinematic motion model of sub-RMM (s) of the ℓth M-EOT, $\widetilde{\boldsymbol{x}}_k^{(\ell,s)} = \left[\left[\boldsymbol{x}_k^{(\ell,s)}\right]^T, \omega_k^{(\ell,s)}\right]^T \in \mathbb{R}^5$ combining the range and velocity $\boldsymbol{x}_k^{(\ell,s)} = \left[p_{x,k}^{(\ell,s)}, p_{y,k}^{(\ell,s)}, \dot{p}_{x,k}^{(\ell,s)}, \dot{p}_{y,k}^{(\ell,s)}\right] \in \mathbb{R}^4$ and the turn rate $\omega_k^{(\ell,s)}$ The maneuvering kinematic motion model is obtained by

$$\boldsymbol{x}_k^{(\ell,s)} = (\boldsymbol{F}_k \otimes \boldsymbol{I}_d)\, \boldsymbol{x}_{k-1}^{(\ell,s)} + \boldsymbol{G}_k\, \boldsymbol{w}_k^{(\ell,s)} \tag{4}$$

where $\boldsymbol{F}_k \in \mathbb{R}^{d_x \times d_x}$ defined the transition matrix, $\boldsymbol{I}_d \in \mathbb{R}^{d \times d}$ is described by the identity matrix, "$\otimes$" stands for Kronecker product, $\boldsymbol{G}_k$ is the matrix of process noise and $\boldsymbol{w}_k^{(\ell,s)} \sim \mathcal{N}\left(0, \boldsymbol{Q}_k^{(\ell,s)}\right)$ is the white process noise with zero mean and covariance $\boldsymbol{Q}_k^{(\ell,s)}$. For the extension $\boldsymbol{\chi}_k^{(\ell,s)}$ the function to explain the extension dynamics in shape, orientation, size, and, in addition to, the measurements distorted from the true extension in shape, size, and orientation. Thus, the dynamic extension model for the state $\left(\boldsymbol{\chi}_k^{(\ell,s)}\right)$ of sub-object s of ℓth M-EOT is obtained as $f_{k|k-1}\left(\boldsymbol{\chi}_k^{(\ell,s)} | \boldsymbol{\chi}_{k-1}^{(\ell,s)}\right) = \mathcal{W}\left(\boldsymbol{\chi}_k^{(\ell,s)}; \delta_k^{(\ell,s)}, \boldsymbol{O}_k^{(\ell,s)} \boldsymbol{\chi}_{k-1}^{(\ell,s)} \left(\boldsymbol{O}_k^{(\ell,s)}\right)^T\right)$, $\boldsymbol{O}_k^{(\ell,s)} \in \mathbb{R}$ is the orientation angle of the ℓth M-EOT, where the invertible matrix $\mathbf{O}_k^{(\ell,s)} \in \mathbb{R}^{d \times d}$ will explain the dependence of the orientation of extension (if $\mathbf{O}_k^{(\ell,s)} = \left(\delta_k^{(\ell,s)}\right)^{-1/2} \begin{bmatrix} \cos\theta & -\sin\theta \\ \sin\theta & \cos\theta \end{bmatrix}$ is the matrix of rotation with angle $\theta = \omega_k T$), T is the sampling time, shape (if $\mathbf{O}_k^{(\ell,s)}$ with other matrix), or size (e.g., $\mathbf{O}_k^{(\ell,s)} = \lambda \boldsymbol{I}_d$), and $\delta_k^{(\ell,s)} > d - 1$ describes the degrees of freedom. $\mathcal{W}(Y; a, C)$ is Wishart distribution' density using Sub-RMM $Y \in \mathbb{S}_{++}^{\mathrm{d}}$, $\mathcal{W}(Y; a, C) = \frac{1}{C} |C|^{-\frac{1}{2}a} |Y|^{\frac{1}{2}(a-d-1)} \mathrm{etr}\left(-\frac{1}{2} C^{-1} Y\right)$ with $\mathrm{a} \geq \mathrm{d}$, where $C = 2^{ad/2} \Gamma[\mathrm{a}/\mathrm{d}]$, $\Gamma[\cdot]$ is multivariate Gamma function, and $\mathrm{etr}(\mathrm{A}) = \exp(\mathrm{Tr}(\mathrm{A}))$ is exponential of tracing matrix.

c. *New ISAR-TBD Observation using Skewed-Sub-RMM*

In this section, we explain a new measurement model of the ISAR image in the TBD approach using sub-RMM and the skewed normal distributions. To cope with the possible abrupt changes of kinematic states, extensions, and measurement distributions over an object when a target manoeuvers. The imaging ISAR observation related to a sub-RMM is explained by using a Gaussian spread function (GSF) with a sub-RMM approximation. We consider that the image frame consists of pre-processed data from the ISAR system for different ranges of sub-RMM $r_k^{(\ell,s)}$, range-rate $\dot{r}_k^{(\ell,s)}$ and azimuthal (rotation) angle $\theta_k^{(\ell,s)} = (\omega_k^{(\ell,s)}\, T)$ bins for sub-RMM (s) of ℓth M-EOT, that means $\widetilde{\boldsymbol{x}}_k^{(\ell,s)} \triangleq \left[r_k^{(\ell,s)}, \dot{r}_k^{(\ell,s)}, \theta_k^{(\ell,s)}\right]^T$. Each ISAR image frame is considered to consist of $(N_r \times N_{\dot{r}} \times N_\theta)$ bins. The resolutions of $r_k^{(\ell,s)}, \dot{r}_k^{(\ell,s)}$ and $\theta_k^{(\ell,s)}$ are denoted by $\Delta_r, \Delta_{\dot{r}}, \Delta_\theta$, respectively. The (a, b, c) th cell for $a = 1, 2, \ldots, N_r$, $b = 1, 2, \ldots, N_{\dot{r}}$, $c = 1, 2, \ldots, N_\theta$, is then centered around $(a\Delta_r \times b\Delta_{\dot{r}} \times c\Delta_\theta)$. Based on these assumptions, the Doppler observation model for ISAR with sub-RMM is defined by $\boldsymbol{z}_k^{(a,b,c)} = \widetilde{\boldsymbol{H}}_k^{(a,b,c)} \widetilde{\boldsymbol{x}}_k^{(\ell,s)} + \boldsymbol{v}_k^{(a,b,c)}$ where $\widetilde{\boldsymbol{H}}_k^{(a,b,c)} = \boldsymbol{H}_k^{(a,b,c)} \otimes \mathbf{I}_d$, $\boldsymbol{H}_k^{(a,b,c)}$ is the nonlinear sub-RMM spread function of $\boldsymbol{x}_k^{(\ell,s)}$, and $\boldsymbol{v}_k^{(a,b,c)}$ is the white Gaussian measurement noise. In [14], the authors introduced a new observation model for a single M-EOT based on a skew normal distributions and RMM approach that is capable of estimating the kinematic state and extension of the EOT with a single ellipse. In this paper, we will improved this model to match with the proposed sub-RMM-TBD approach and ISAR images tracking for multiple M-EOTs. In [14], the skew normal distribution using the random vector z with $p(z) = p(\mathcal{Y} | \varphi > 0)$, where $\mathcal{Y}$ is a p -dimensional random vector with its probability density function (PDF) given by $p(\mathcal{Y}) = \mathcal{N}(\mathcal{Y}; \mu, \Sigma)$ and φ is an $\boldsymbol{m}$ -dimensional random vector. The distribution of z is $p(z) = [P\{\varphi > 0\}]^{-1} \mathcal{N}(\boldsymbol{z}; \mu, \Sigma) P\{\varphi > 0 | \mathcal{Y} = y\}$, where $P\{D\}$ is the probability of the event D. Let's consider a particular case of $\boldsymbol{m} = 1$ then $p(\mathcal{Y}) = \mathcal{N}(\mathcal{Y}; \mu + \beta\, \varphi, \Sigma)$ and $p(\varphi) = \mathcal{TN}\left(\varphi; \xi, \eta, (0, \infty)\right)$, where β is $p \times 1$ vector of constraint, φ is a random scalar, $\mathcal{TN}\left(\xi, \eta, (\mathfrak{a}, \mathfrak{b})\right)$ defined a truncated normal distribution on $(\mathfrak{a}, \mathfrak{b})$. This paper considers the following observation model for ISAR skewed-TBD-sub-RMM,

$$\boldsymbol{z}_k^{(a,b,c)} \triangleq \begin{cases} \displaystyle\sum_{\ell=1}^{N(k)} \sum_{s=1}^{n_k^{(\ell,s)}} \Upsilon_x^{(\ell,s)} \widetilde{\boldsymbol{H}}_k^{(a,b,c)} \begin{bmatrix} r_k^{(\ell,s)} \\ \dot{r}_k^{(\ell,s)} \\ \theta_k^{(\ell,s)} \end{bmatrix} + \boldsymbol{v}_k^{(a,b,c)}, & \boldsymbol{H}_1 \\ \boldsymbol{v}_k^{(a,b,c)}, & \boldsymbol{H}_0 \end{cases},$$

$$p\left(\boldsymbol{v}_k^{(a,b,c)} \middle| \varphi_k^{(\ell,s)}, \boldsymbol{\chi}_k^{(\ell,s)}\right) \cong \mathcal{N}\left(\beta_k^{(\ell,s)} \varphi_k^{(\ell,s)}, \boldsymbol{B}_k^{(\ell,s)} \boldsymbol{\chi}_k^{(\ell,s)} \left(\boldsymbol{B}_k^{(\ell,s)}\right)^T\right),$$

$$p\left(\varphi_k^{(\ell,s)}\right) \sim \mathcal{TN}\left(\xi_k^{(\ell,s)}, \left(\eta_k^{(\ell,s)}\right)^2, (0, \infty)\right)$$

$$\cong \frac{1}{\left[1 - \Phi\left(-\xi_k^{(\ell,s)} / \eta_k^{(\ell,s)}\right)\right] \sqrt{2\pi \eta_k^{(\ell,s)}}} \exp\left[-\frac{\left(\varphi_k^{(\ell,s)} - \xi_k^{(\ell,s)}\right)^2}{2\left(\eta_k^{(\ell,s)}\right)^2}\right] \tag{5}$$

where $\boldsymbol{H}_1$ means if there are $N(k)$ M-EOTs present and $\boldsymbol{H}_0$ denoting if there no M-EOTs, $\Upsilon_x^{(\ell,s)}$ is the complex amplitude of sub-RMM (s) of the ℓth M-EOT, the white Gaussian measurement noise cell, $\boldsymbol{v}_k^{(a,b,c)}$ is with PDF related to the observation covariance matrix $\left(\boldsymbol{R}_k^{(a,b,c)}\right)$ and $p\left(\boldsymbol{v}_k^{(a,b,c)} \middle| \varphi_k^{(\ell,s)}, \boldsymbol{\chi}_k^{(\ell,s)}\right) \sim \mathcal{N}\left(\boldsymbol{v}_k^{(a,b,c)}; \beta_k^{(\ell,s)} \varphi_k^{(\ell,s)}, \lambda\, \boldsymbol{\chi}_k^{(\ell,s)} + \boldsymbol{R}_k^{(a,b,c)}\right)$. Here $\boldsymbol{v}_k^{(a,b,c)}$ is following a white Gaussian noise with $\boldsymbol{R}_k^{(a,b,c)}$ given by $\boldsymbol{\chi}_k^{(\ell,s)}$ and $\boldsymbol{B}_k^{(\ell,s)} \Lambda$ is a scalar effect of $\boldsymbol{\chi}_k^{(\ell,s)}$. Therefore, $\boldsymbol{v}_{\mathrm{k}}^{(a,b,c)}$ can be approximated by considering $\boldsymbol{B}_k^{(\ell,s)} = \left(\lambda\, \boldsymbol{\chi}_k^{(\ell,s)} + \boldsymbol{R}_k^{(a,b,c)}\right)^{1/2} \left(\boldsymbol{\chi}_k^{(\ell,s)}\right)^{-1/2}$ which explains the distortion of the extension from the real one in shape, size, and orientation. $\beta_k^{(\ell,s)}$ is $d \times 1$ vector of constraint, and $\varphi_k^{(\ell,s)}$ is a truncated Gaussian distributed random variable, for $\varphi_k^{(\ell,s)} \in [0, +\infty)$, $\Phi(\bullet)$ represents the standard normal distribution function, and

$$\varphi_k^{(\ell,s)} = \rho_k^{(\ell,s)} \varphi_{k-1}^{(\ell,s)} + \psi_k^{(\ell,s)} \tag{6}$$

where $\rho_k^{(\ell,s)} = \hat{\chi}_{k|k-1}^{(\ell,s)} / \hat{\chi}_{k-1}^{(\ell,s)}$ denoted the transition factor of sub-RMM (s) of the ℓth M-EOT and $\psi_k^{(\ell,s)} \sim \mathcal{TN}\left(\psi_k^{(\ell,s)}; 0, \left(K_k^{(\ell,s)}\right)^2, (0,+\infty)\right)$ is the process noise. The contribution of the proposed ISAR skewed-TBD-sub-RMM Doppler observation model is its ability to effectively describe the skewed distribution of Doppler observations using a simple random variable $\beta_k^{(\ell,s)} \varphi_k^{(\ell,s)}$. The vector $\beta_k^{(\ell,s)}$ describes the skewness direction and latent variable $\varphi_k^{(\ell,s)}$ defined how large is the skewness. For M-EOT, the vector $\beta_k^{(\ell,s)}$ defined the skewness direction will be determined as $\beta_k^{(\ell,s)} = \left[\cos\theta_k^{(\ell,s)} \quad \sin\theta_k^{(\ell,s)}\right]^T$, where $\theta_k^{(\ell,s)}$ is the skewness direction' angle. Fig. 2(right) shows example of $\boldsymbol{v}_k^{(a,b,c)}$ for M-EOT with different values of $\beta_k^{(\ell,s)}$.

3 Skewed Sub-RMM-TBD Multi-Bernoulli Filter

In this section, on the basis of the multi-Bernoulli (MB) filter for EOTs proposed in [9], we will explain the closed-form expressions for an updated recursive Skewed (SK)-Sub-RMM-MB-TBD filter. The conventional MB-EOT filtering algorithm proposed in [9] has proved that if π_{k-1} is MB-EOT, the predicted multi-target density $\pi_{k|k-1}$ is MB-EOT, then the updated multi-target density π_k is also an MB-EOT under the assumption that the extents of the targets in the surveillance region are small and the targets do not overlap. Based on these approximations, the joint prior SK-Sub-RMM-MB-TBD distribution of the state $\boldsymbol{\xi}_k^{(\ell,s)} \triangleq \left(\boldsymbol{x}_k^{(\ell,s)}, \boldsymbol{\chi}_k^{(\ell,s)}\right)$ hybrid with the skewness parameter $\varphi_k^{(\ell,s)}$ that combination of multiple sub-objects $n_{k-1}^{(\ell,s)}$ of the ℓth M-EOT at time $k-1$ is specified as

$$\pi_{k-1} = \left\{\left\{r_{k-1}^{(\ell,s)}, p_{k-1}^{(\ell,s)}(\boldsymbol{\xi}_{k-1}; \varphi_{k-1})\right\}_{s=1}^{n_{k-1}^{(\ell,s)}}\right\}_{\ell=1}^{M_{k-1}} \tag{7}$$

where $r_{k-1}^{(\ell,s)}$ is the probability of existence and $p_{k-1}^{(\ell,s)}(.)$ is state distribution of sub-object s of ℓth SK-Sub-RMM-MB-TBD component for each M-EOT. M_{k-1} defines the hypothesized track number at time $k-1$.

<u>SK-Sub-RMM-MB-TBD Prediction:</u> Given the posterior SK-Sub-RMM-MB-TBD parameters π_{k-1} at time -1, the predicted SK-Sub-RMM-MB-TBD parameters are

$$\pi_{k|k-1} = \left\{\left\{r_{P,k|k-1}^{(\ell,s)}, p_{P,k|k-1}^{(\ell,s)}(\boldsymbol{\xi}_k; \varphi_k)\right\}_{s=1}^{n_k^{(\ell,s)}}\right\}_{\ell=1}^{M_{k-1}} \cup \left\{\left\{r_{\Gamma,k}^{(\ell,s)}, p_{\Gamma,k}^{(\ell,s)}(\boldsymbol{\xi}_k; \varphi_k)\right\}_{s=1}^{n_k^{(\ell,s)}}\right\}_{\ell=1}^{M_{\Gamma,k}} \tag{8}$$

where $r_{P,k|k-1}^{(\ell,s)} = r_{k-1}^{(\ell,s)} \langle p_{k-1}^{(\ell,s)}(\boldsymbol{\xi}_{k-1}; \varphi_{k-1}), p_{s,k}(\boldsymbol{\xi}_{k-1}; \varphi_{k-1})\rangle$,

$$p_{P,k|k-1}^{(\ell,s)}(\boldsymbol{\xi}_k; \varphi_k) = \frac{\langle f_{k|k-1}(\boldsymbol{\xi}_k, \varphi_k | \cdot), p_{k-1}^{(\ell,s)}(\boldsymbol{\xi}_{k-1}; \varphi_{k-1}) p_{s,k}(\boldsymbol{\xi}_{k-1}; \varphi_{k-1})\rangle}{\langle p_{k-1}^{(\ell,s)}(\boldsymbol{\xi}_{k-1}; \varphi_{k-1}), p_{s,k}(\boldsymbol{\xi}_{k-1}; \varphi_{k-1})\rangle},$$

$$f_{k|k-1}(\boldsymbol{\xi}_k, \varphi_k | \cdot) = f_{\boldsymbol{x},k|k-1}(\boldsymbol{x}_k | \boldsymbol{x}_{k-1})\, f_{\boldsymbol{\chi},k|k-1}(\boldsymbol{\chi}_k | \boldsymbol{\chi}_{k-1})\, f_{\varphi,k|k-1}(\varphi_k | \varphi_{k-1}).$$

where $f_{k|k-1}(\boldsymbol{\xi}_k, \varphi_k | \cdot)$ is the transfer function at time k, for the jointed state with tracking parameters such as $\boldsymbol{x}_k, \boldsymbol{\chi}_k$ and φ_k. $\cup$ is the union symbol, $p_{s,k}$ is the probability of survival, $\left(r_{\Gamma,k}^{(\ell,s)}, p_{\Gamma,k}^{(\ell,s)}\right)$are parameters of an SK-Sub-RMM-MB-TBD for birth M-EOTs at time k, where $\langle\cdot,\cdot\rangle$ explain the operation of the inner product. The predicted hypothesized' number is $M_{k|k-1} = M_{k-1} + M_{\Gamma,k}$. Based on (6), $f_{\varphi,k|k-1}(\varphi_k | \varphi_{k-1}) = \mathcal{TN}\left(\varphi_k; \hat{\xi}_{P,k|k-1}, \hat{\eta}_{P,k|k-1}^2, (0,\infty)\right)$ with$\hat{\xi}_{P,k|k-1} = \rho_k \hat{\xi}_{k-1}$, $\hat{\eta}_{P,k|k-1}^2 = \rho_k^2\ \hat{\eta}_{k-1}^2 + K_k^2$.

<u>SK-Sub-RMM-MB-TBD Update</u>: Assume that the predicted density of M-EOTs is an SK-Sub-RMM-MB-TBD with parameter $\pi_{k|k-1} = \left\{\left\{r_{k|k-1}^{(\ell,s)}, p_{k|k-1}^{(\ell,s)}(\boldsymbol{\xi}_k; \varphi_k)\right\}_{s=1}^{n_k^{(\ell,s)}}\right\}_{\ell=1}^{M_{k/k-1}}$.

Since the origins of an M-EOT measurement are only partially resolvable, we also assume that no further information is available about the correspondences between sub-objects and measurements set $\mathbf{Z}_k$; and the measurement can be obtained from any possible sub-object. Then, the posterior density at time k can be approximated as

$$\pi_k \cong \left\{\left\{\left\{\left(r_k^{(\ell,s)}, p_k^{(\ell,s)}\left(\boldsymbol{\xi}_k | \boldsymbol{W}_k^{(\mathcal{P},j)}; \varphi_k\right)\right)\right\}_{\boldsymbol{W}_k^{(\mathcal{P},j)} \in \wp_k^{(\mathcal{P})} \angle \mathbf{Z}_k}\right\}_{s=1}^{n_k^{(\ell,s)}}\right\}_{\ell=1}^{M_{k|k-1}}$$
$$, j = 1, \cdots, \left|\wp_k^{(\mathcal{P})}\right|, \mathcal{P} = 1, \cdots, \boldsymbol{N}_{\wp,k} \tag{9}$$

where $\wp_k^{(\mathcal{P})}$ is the $\mathcal{P}th$ partition of the measurement set $(\mathbf{Z}_k)$, $\boldsymbol{W}_k^{(\mathcal{P},j)} \in \wp_k^{(\mathcal{P})}$ is the j th cell of partition $\wp_k^{(\mathcal{P})}$, $\left|\wp_k^{(\mathcal{P})}\right|$ is the number of cells from $\wp_k^{(\mathcal{P})}$ and $\boldsymbol{W}_k^{(\mathcal{P},j)}$ does not include null set; $\boldsymbol{N}_{\mathcal{P},k}$ is the number of partitions at time step k, the notation $\wp_k^{(\mathcal{P})} \angle \mathbf{Z}_k$ is the partitioning shorthand that means $\wp_k^{(\mathcal{P})}$ to partition the measurement set $\mathbf{Z}_k$ into non-empty cells $\boldsymbol{W}_k^{(\mathcal{P},j)}$. During this paper, the mean of a known cell $\boldsymbol{W}_k^{(\mathcal{P},j)}$ is calculated by (10-11) in an appendix. Furthermore, a Sequential Monte Carlo (SMC) implementation is applied to estimate non-Linear kinematic M-EOTs state. The proposed algorithm is implementation using SMC technique, which obtains higher estimation accuracy than other filters, as the SMC-MB-TBD filter does not need the extra clustering method to extract M-EOTs states.

4 Numerical Results

During this section, we will demonstrate the performance of the proposed SK-Sub-RMM-MB-TBD filter for M-EOTs in a TBD application and compare the results with H-PMHT-TBD [8] and MM-One ellipse (RMM)-MB [1] filters. As in many actual ISARs, the signal transmitted by the radar is generated by Chirp or linear frequency modulation and is convolved with the impulse response of ISAR on the time domain, and the AWGN noise is added to it. The values of the radar's main parameters are presented in [11]. The size and shape of the M-EOTs are similar to DJI Inspire 1 and DJI Phantom 2. To evaluate the performances of the filters, we assessed location and the extent errors simultaneously with a

single score by means of the Gaussian Wasserstein distance (GWD) [15]. The GWD compares two ellipses according to (12) in an appendix. In this case, the first ellipse is the ground truth, and the second one is the extended object tracking method estimate. The following parameters were used to generate ISAR data: $T = 1\,s$, $\theta = 1\,s$. The simulation uses a maximum of $L_{max} = 5000$ particles per hypothesized and $L_{min} = 1000$ particles. We consider a two-dimensional scenario over 400 × 600 resolution cells with cell length $\Delta_x = \Delta_x = 1$ m. Up to 4 M-EOTs are included in the scenario whose trajectories during the entire surveillance period (K = 45 frames, frame interval is 3 s) are shown in Fig. 3 . Three models are considered in simulations with different known turn rates. The survival probability for actual targets is $p_{S,k} = 0.99$. We considered a realistic radar resolution of 2.5 m in range, $2\frac{m}{s}$ in Doppler, and 1 deg in azimuth. Since the observation array is an image, the array index will be treated as an ordered pair of integers $i = (a, b)$. The blurring factor $\sigma_h^2 = 1$, and $(p_{x,k}, p_{y,k})$ being the position of the state x_k. A typical observation and real M-EOTs trajectories are shown in Fig. 3. At each time step in the proposed SK-Sub-RMM-MB-TBD and other filters, pruning and merging of an increased number of components are performed for each hypothesized track with a threshold $T_{merge} = 0.75$ times the pixel width. Tracks with existence probabilities less than $r = 10^{-2}$are dropped, and a maximum of $T_{max} = 100$ tracks are kept.The birth process is an MB RFS with density: $\pi_{\Gamma,k} = \left\{\left(r_{\Gamma,k}^{(i)}, p_{\Gamma,k}^{(i)}\right)\right\}_{i=1}^{4}, r_{\Gamma,k}^{(1)}, r_{\Gamma,k}^{(2)}, r_{\Gamma,k}^{(3)}, r_{\Gamma,k}^{(4)} = .02$ $, P_{\Gamma,k}^{(i)}(x) w_{\Gamma,k}^{(i)} N\left(; m_{\Gamma,k}^{(i)}, p_{\Gamma,k}^{(i)}\right)$where the mean matrices m are the initial true states of 4 targets. The 100 Monte Carlo runs are achieved, the results are shown in Figs. 4 (a)-(d). They show that the new algorithm can solve the M-EOTs problem. The simulation results demonstrate the effectiveness of the proposed new algorithm using skewness-Sub-RMM-TBD. The sample images from a scenario simulation with low and high noise effect are shown in Figs. 4(a) and 4(b). As shown in fig 4(a), the proposed filter can obtain detailed extension information about size, shape, and orientation, while the other filters only can approximate the extension by using an ellipsoid (almost a circle) without shape and orientation information. The results of different filters with high noise effects are shown in Fig. 4(b). There is a downward trend while M-EOTs are maneuvering.

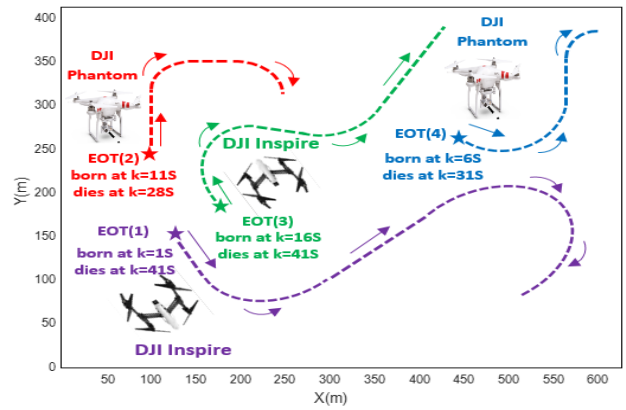

Fig.3. True M-EOTs tracks in $x - y$ plane.

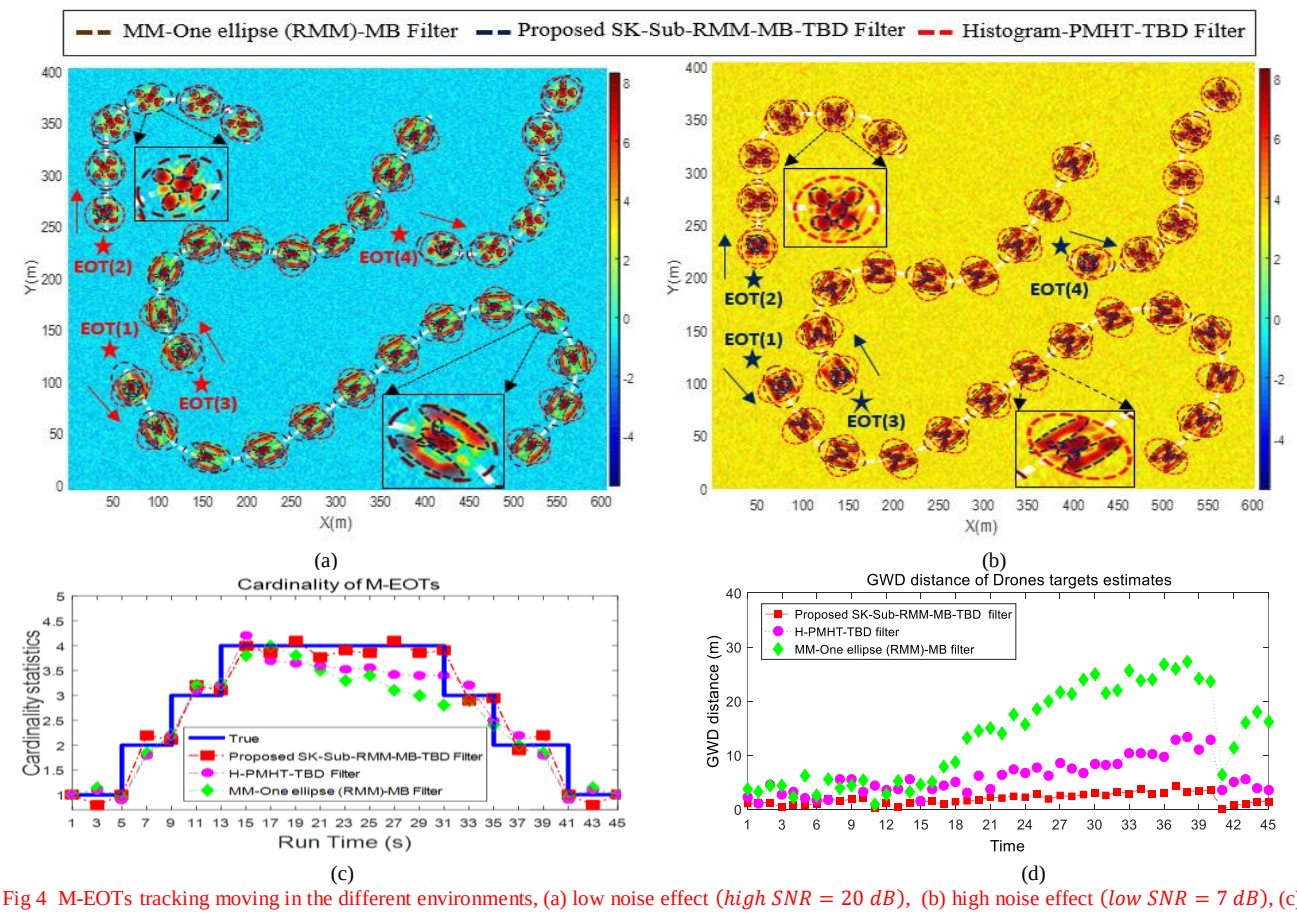

Fig 4 M-EOTs tracking moving in the different environments, (a) low noise effect ($high\ SNR = 20\ dB$), (b) high noise effect ($low\ SNR = 7\ dB$), (c) Mean cardinality estimate, (d) Mean GWD estimate

The reason is that other filters false to have the extension estimation. The measurements are typically treated as one M-EOT through the other filters. The performance GWD and cardinality are shown in Fig. 4(c), (d). The proposed algorithm performs well without errors. The computational complexity of the proposed algorithm is approximately $\mathcal{O}(N_{z,k}^2)$, $N_{z,k} \triangleq (N_r \times N_{r^{\cdot}} \times N_\theta)$.

5 Conclusion

In this paper, we consider the problem of multi-manoeuvering EOTs tracking from ISAR images. We proposed an SK-Sub-RMM-MB-TBD filter to improve the extent state estimation of manoeuvering EOTs. We address a joint detection and tracking of M-EOTs. We introduce a skewness-Sub-RMM-MB-TBD composed of sub-ellipses; each one is represented by an RMM, which is used to estimate maneuvering kinematic states and extensions of sub-objects for each M-EOTs. Simulations have verified the theoretical results.

6 References

[1] Jiang, T., Liu, M., Fan, Z., Zhang, S.: 'On multiple-model extended target multi-Bernoulli filters', Digital Signal Processing 2016, 59, pp.76–85.

[2] Lei C., Lingjiang K., Suqi L., Wei Y., "The multiple model multi-Bernoulli filter based track-before-detect using a likelihood based adaptive birth distribution", *Signal Processing*, Vol. 171, 2020, pp.107501

[3] Y. Wei, Fang Zicheng, Li Wujun, "Multi-Frame Track-Before-Detect Algorithm for Maneuvering Target Tracking", *IEEE Trans. Veh. Tech.*, vol. 69, no.4, pp. 4104- 4118, 2020.

[4] Lan, J., Li, X R.: 'Tracking of Maneuvering Non-Ellipsoidal Extended Object or Target Group Using Random Matrix' IEEE Trans. Signal Process, 2014, 62, (9), pp. 2450– 2463.

[5] Liang, Z., Liu, F., Gao, J.: 'Improved GGIW-PHD filter for maneuvering non-ellipsoidal extended targets or group targets tracking based on sub-random matrices', PLoS One, 2018, 13, (2), pp.1-28.

[6] L. Sun, H. Yu, Z. Fu, Z. He and J. Zou, "Modeling and Tracking of Maneuvering Extended Object With Random Hypersurface,", *IEEE Sensors Journal*, vol. 21, no. 18, pp. 20552-20562, 2021

[7] S. F. KARA, ÖZKAN E., "Multiellipsoidal extended target tracking with known extent using sequential Monte Carlo framework", *Turkish Journal of Electrical Engineering and Computer Sciences*, vol. 27, no.2, PP.1546-1558, 2019.

[8] Wieneke, M., Davey, S.: 'Histogram-PMHT for Extended Targets and Target Groups in Images', IEEE Trans. Aerospace and Electronic Systems, 2014, 50, (3), pp. 2199 – 2217.

[9] M. Barbary, Mohamed H. Abd ElAzeem. "Multiple extended stealth target tracking from image observation based on non-linear sub-random matrices approach,", *IET Radar, Sonar & Navigation*, vol. 15, pp. 274–293, 2021.

[10] Errasti-Alcala, B., Braca, P.: 'Track before Detect Algorithm for Tracking Extended Targets Applied to Real-World Data of X-Band Marine Radar', In Proceedings of the 2014 17th International Conference, Information Fusion (FUSION), Salamanca, Spain, 7 – 10 July 2014.

[11] S.-J. Lee, Lee M.-J., Kim K.-T., Bae J.-H., "Classification of ISAR images using variable cross-range resolutions", *IEEE Trans. Aerosp. Electron. Syst.*, vol. 54, no.5, pp. 2291–2303, 2018.

[12] C. J. Li, and Hao Ling, "Wide-Angle, Ultra-Wideband ISAR Imaging of Vehicles and Drones", *Sensors*, vol. 18, no. 3331, pp.1-15, 2018.

[13] Li CJ and Ling H., "An investigation on the radar signatures of small consumer drones", *IEEE Antennas Wirel. Propag. Lett.*, vol. 16, pp.649–652, 2016.

[14] L. Zhang and J. Lan, "Extended Object Tracking Using Random Matrix With Skewness," in *IEEE Transactions on Signal Processing*, vol. 68, pp. 5107-5121, 2020

[15] S. Yang, M. Baum, and K. Granström, "Metrics for performance evaluation of elliptic extended object tracking methods" in Proc. 2016 IEEE Int. Conf. Multisensor Fusion Integr. Intell. Syst., Baden-Baden, Germany, pp. 523–528, 201.

Table 1 Average running time for single Monte Carlo, s

Proposed SK-Sub-RMM-MB-TBD	H-PMHT-TBD	MM-One ellipse (RMM)-MB
30.56	55.34	32.93

The average 100 Monte Carlo runs for the recent algorithms is reported in Table 1. It is apparent that proposed robustness filter outperforms all filters and has the best real-time performance.

Appendix

The mean of a known cell $\boldsymbol{W}_k^{(\mathcal{P},j)}$ is calculated by

$$\bar{\boldsymbol{z}}_k^{(\mathcal{P},j)} \triangleq \frac{1}{\left|\boldsymbol{W}_k^{(\mathcal{P},j)}\right|}\sum_{\tilde{\boldsymbol{z}}_k^{(a,b,c)} \in \boldsymbol{W}_k^{(\mathcal{P},j)}} \tilde{\boldsymbol{z}}_k^{(a,b,c)},$$

$$j = 1,\cdots,\left|\wp_k^{(\mathcal{P})}\right|, \quad \mathcal{P} = 1,\cdots,\boldsymbol{N}_{\wp,k},$$

where $\left|\boldsymbol{W}_k^{(\mathcal{P},j)}\right|$ denoted by the cell observations number. The updated MB filter, in the same cases, requires a likelihood of measurements in each cell $\boldsymbol{W}_k^{(\mathcal{P},j)}$. Thus, the pseudo-likelihood of sub-object s is a function of $\left(\boldsymbol{W}_k^{(\mathcal{P},j)}, \boldsymbol{\xi}_k^{(\ell,s)}, \varphi_k^{(\ell,s)}\right)$ and given by (8). Thus, the updated MB parameters are

$$r_k^{(\ell,s)} = \frac{w_{\wp^{(\mathcal{P})}}}{d\boldsymbol{W}_k^{(\mathcal{P},j)}}.$$

$$\frac{r_{k|k-1}^{(\ell,s)}\langle p_{k|k-1}^{(\ell,s)}(\boldsymbol{\xi}_k;\ \varphi_k), \mathcal{L}_{\boldsymbol{W}_k^{(\mathcal{P},j)}}(\boldsymbol{\xi}_k;\ \varphi_k)\rangle}{1 - r_{k|k-1}^{(\ell,s)} + r_{k|k-1}^{(\ell,s)}\langle p_{k|k-1}^{(\ell,s)}(\boldsymbol{\xi}_k;\ \varphi_k), \mathcal{L}_{\boldsymbol{W}_k^{(\mathcal{P},j)}}(\boldsymbol{\xi}_k;\ \varphi_k)\rangle},$$

$$p_k^{(\ell,s)}\left(\boldsymbol{\xi}_k | \boldsymbol{W}_k^{(\mathcal{P},j)}, \varphi_k\right) = \frac{p_{k|k-1}^{(\ell,s)}(\boldsymbol{\xi}_k, \varphi_k)\, \mathcal{L}_{\boldsymbol{W}_k^{(\mathcal{P},j)}}(\boldsymbol{\xi}_k, \varphi_k)}{\langle p_{k|k-1}^{(\ell,s)}(\boldsymbol{\xi}_k, \varphi_k), \mathcal{L}_{\boldsymbol{W}_k^{(\mathcal{P},j)}}(\boldsymbol{\xi}_k, \varphi_k)\rangle},$$

$$\boldsymbol{d}_{\boldsymbol{W}_k^{(\mathcal{P},j)}} = \delta_{1,\left|\boldsymbol{W}_k^{(\mathcal{P},j)}\right|} + \sum_{\ell=1}^{M_{k/k-1}}\sum_{s=1}^{n_k^{(\ell,s)}} \frac{r_{k|k-1}^{(\ell,s)}\langle p_{k|k-1}^{(\ell,s)}(\boldsymbol{\xi}_k, \varphi_k), \mathcal{L}_{\boldsymbol{W}_k^{(\mathcal{P},j)}}(\boldsymbol{\xi}_k, \varphi_k)\rangle}{1 - r_{k|k-1}^{(\ell,s)} + r_{k|k-1}^{(\ell,s)}\langle p_{k|k-1}^{(\ell,s)}(\boldsymbol{\xi}_k, \varphi_k), \mathcal{L}_{\boldsymbol{W}_k^{(\mathcal{P},j)}}(\boldsymbol{\xi}_k, \varphi_k)\rangle} \quad (10)$$

where $\mathcal{L}_{\boldsymbol{Z}_k}\left(\boldsymbol{\xi}_k^{(\ell,s)}; \varphi_k^{(\ell,s)}, \Upsilon_k\right)$ is the sub-RMM' likelihood function condition on $\varphi_k^{(\ell,s)}$ which is given by

$$\mathcal{L}_{\boldsymbol{Z}_k}\left(\boldsymbol{\xi}_k^{(\ell,s)}; \varphi_k^{(\ell,s)}, \Upsilon_k\right) = e^{-\gamma\left(\xi_k^{(\ell,s)}\right)}\gamma\left(\boldsymbol{\xi}_k^{(\ell,s)}\right) \prod_{\substack{a,b,c \in \left(\xi_k^{(\ell,s)}\right): \\ \xi_k^{(\ell,s)} \in \boldsymbol{X}_k}} \frac{\boldsymbol{\Psi}\left(\boldsymbol{z}_k^{(a,b,c)} | \boldsymbol{\xi}_k^{(\ell,s)}; \varphi_k^{(\ell,s)}\right)}{\boldsymbol{\Phi}\left(\boldsymbol{z}_k^{(a,b,c)}\right)} \quad (11)$$

where $\gamma(\cdot)$ is predicted number of observations obtained by a sub-RMM, and is considered to be a function of sub-RMM' volume [9]; the quantities $w_{\wp_k^{(\mathcal{P})}}$ and $\boldsymbol{d}_{\boldsymbol{W}_k^{(\mathcal{P},j)}}$ are, respectively, non-negative coefficients of the partition $\wp_k^{(\mathcal{P})}$ and cell $\boldsymbol{W}_k^{(\mathcal{P},j)}$, $\delta_{\hbar,g}$ is the Kronecker delta function (i.e., if $\hbar = g$, $\delta_{\hbar,g} = 1$; otherwise, $\delta_{\hbar,g} = 0$).

The GWD of two ellipses

$$\Lambda_{GWD}\left(\boldsymbol{\xi}_k^{(j,s)}, \hat{\boldsymbol{\xi}}_k^{(i,s)}\right) = \left\|\boldsymbol{h}_k \boldsymbol{x}_k^{(j,s)} - \boldsymbol{h}_k \hat{\boldsymbol{x}}_k^{(i,s)}\right\|^2 + \mathrm{Tr}\left(\boldsymbol{\chi}_k^{(j,s)} + \hat{\boldsymbol{\chi}}_k^{(i,s)} - 2\sqrt{\sqrt{\boldsymbol{\chi}_k^{(j,s)}}\ \hat{\boldsymbol{\chi}}_k^{(i,s)}\ \sqrt{\boldsymbol{\chi}_k^{(j,s)}}}\right) \quad (12)$$